



Monitoring-based evaluation of dynamic characteristics of a long span suspension bridge under typhoons

Jian Guo¹ · Cheng-Jie Hu¹ · Min-Jun Zhu¹ · Yi-Qing Ni²

Received: 31 July 2020 / Revised: 16 November 2020 / Accepted: 6 December 2020 / Published online: 10 February 2021
© Springer-Verlag GmbH Germany, part of Springer Nature 2021

Abstract

The Xihoumen Bridge, with a main span of 1650 m and two side spans of 578 m and 485 m, respectively, is a long-span suspension bridge spanning the Jintang and Cezi islands in Zhejiang Province, China. In order to establish a reference baseline for vibration mitigation and condition assessment of the bridge under typhoons, the wind field properties, vibration energy distribution, and modal parameters of the bridge are identified through in-situ monitoring. Dynamic responses at different locations on main span and wind speeds at 1/2 main span of the bridge under 10 typhoons and under normal wind were collected for this study. Vibration energy distribution is estimated using wavelet packet transform. Modal parameters are identified by the peak-picking (PP) and data-driven stochastic subspace identification (SSI-DATA) methods. The results indicate that in the low-frequency range, the fluctuating wind energy of typhoons changes more significantly than that of normal wind. More than 80% of the vibration energy is concentrated in the frequency band (0–1.5625 Hz) under typhoons, while nearly 90% of the vibration energy under normal winds is evenly distributed in three frequency bands (0–1.5625 Hz, 1.5625–3.125 Hz, and 3.125–4.6875 Hz). When using typhoon-induced dynamic responses as input, the SSI-DATA method performs better than the PP method in the identification of modal parameters. The results obtained in this study can be used as a baseline for future structural condition assessment of the bridge after typhoon events.

Keywords Long span suspension bridge · Monitoring system · Typhoon · Vibration energy distribution · Modal frequency · Damping ratio

1 Introduction

Typhoon is one of the most severe natural disasters in some coastal regions, with high frequency of occurrence, long duration of action, and wide range of influence. It often brings threats to human life, causes economic losses [1–4], and affects structural performance of high-rise buildings and spatial structures [5–7]. According to the historical data, there were about seven typhoons on average landing in China each year and most of them occurred at the eastern coast [1, 8]. Since long-span cable-supported bridges comprise flexible and slender components, they are susceptible

to external wind excitations. For coastal regions, the impact of typhoons is more significant due to the lack of land cover, which brings greater challenges to bridge safety.

The relationship among the wind excitation, vibration response, and modal parameters of a long-span bridge is critical for the assessment of typhoon-induced risk. The vibration energy distribution in different frequency bands can help understand the wind-induced dynamic response characteristics of a bridge, while modal parameters represent the inherent dynamic characteristics of the bridge. As a result, the vibration energy distribution analysis and modal parameter identification of long-span bridges can provide baseline information for structural vibration suppression, health condition assessment, and reliability evaluation.

Many scholars have conducted investigations on vibration energy distribution evaluation and modal parameter identification of bridges. For wavelet-based vibration energy evaluation, the wavelet packet energy spectrum (WPES) was extracted using wavelet packet analysis from the measured dynamic responses caused by ambient excitations [9]. Ge

✉ Jian Guo
guoj@zjut.edu.cn

¹ Institute of Bridge Engineering, Zhejiang University of Technology, Hangzhou 310023, China

² Department of Civil and Environmental Engineering, The Hong Kong Polytechnic University, Hung Hom, Kowloon, Hong Kong

and Li [10] proposed the wavelet packet energy accumulated variation index to detect structural damage in reliance on its ability to capture the change of energy distribution in frequency band. Wei et al. [11] proposed a method for extracting structural damage information and identifying structural damage based on the wavelet packet energy. In their study, the load was applied to a concrete slab, and the structural health status was determined by the energy change of each frequency band of the acceleration data. Based on experiment and finite element simulation (FEM), Guo and He [12] investigated the energy distribution of ship collision with bridge pier by using wavelet packet analysis and obtained dynamic features of structural response under different impact forces. Pan et al. [13] defined energy ratio deviation (ED) and energy ratio variance (EV) through the analysis of acceleration response signals by means of wavelet packet and obtained the baseline threshold for structural damage warning.

In the field of modal parameter identification of bridges, Peeters et al. [14] and Ren et al. [15, 16] used the SSI-DATA method to identify the modal parameters of structural systems of different orders. Weng et al. [17] and Jang et al. [18] addressed output-only modal identification of bridges instrumented with wireless monitoring systems. Zarbaf et al. [19] adopted the covariance-driven stochastic subspace identification (SSI-COV) method to identify the modal properties of a cable-stayed bridge. Mao et al. [20] and Wang et al. [21] pursued automated modal parameter identification of bridges using dynamic response monitoring data collected during typhoons, where the correlation between the modal parameters and environmental factors (temperature and wind speed) was studied. The peak picking (PP) method was utilized for modal parameter identification as well [22, 23]. Zong et al. [24] used the PP method to identify the natural frequencies of a long-span prestressed concrete continuous rigid frame bridge. Ye et al. [25] applied the PP method to identify the modal parameters of a suspension bridge. In addition, a wavelet transform method was adopted to identify the modal parameters of a cable-stayed bridge under typhoons [26]. Sun et al. [27] derived the characteristic of the response transfer ratio that is equivalent to the mode ratio and is independent of the input at the poles of a system. The mode ratio was estimated by singular value decomposition (SVD) and transfer ratio vector, from which the modal parameters of the system were determined. Zong et al. [28] used the monitoring data acquired by accelerometers, temperature sensors, and anemometers installed on an arch bridge with a main span of 636.6 m to conduct modal analysis. On the premise of eliminating the environmental factors such as temperature, vehicle load, and wind excitation, the nonlinear principal component analysis method and artificial neural network model were used to process the data, and finally a modal coefficient correction technique was proposed. Wen

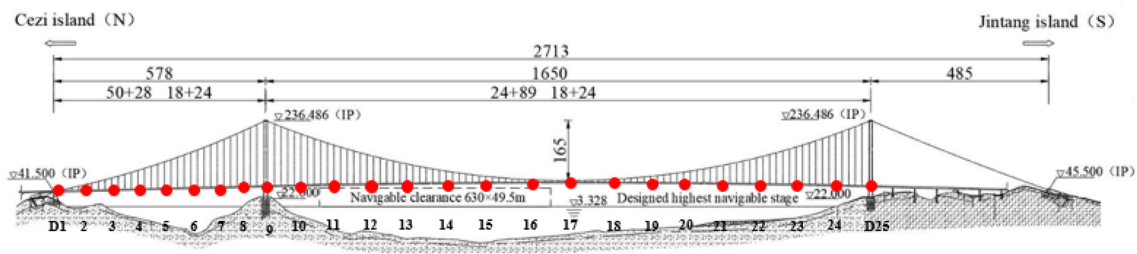
et al. [29] proposed a true modal screening algorithm based on preliminarily estimated modal parameters and applied the algorithm to a cable-stayed bridge with a main span of 1088 m. With the acceleration data collected in 4 months, the stability diagrams were drawn and the modal parameters of the first ten modes were identified. Eshkevari et al. [30] proposed a modal identification method for bridges using the data collected from a mobile vehicle network. When the instrumented vehicle moved on a bridge, the built-in sensor scanned the vibration of the bridge in space and time to obtain a large amount of data, and subsequently constructed a dense matrix from the observations using alternating least squares (ALS), with which the modal parameters of the bridge were identified.

The above investigations provide good references for vibration energy analysis and modal parameter identification of long-span bridges in operational condition. In the present study, we endeavor to understand the vibration energy distribution characteristics of a long-span suspension bridge (the Xihoumen Bridge with a main span of 1650 m) in different frequency bands by exploring ten typhoons and normal monsoon winds and to identify the modal parameters under strong winds with the purpose of providing a reference baseline for post-hazard bridge health assessment in the future. To this end, using the measured acceleration and wind data acquired by a structural health monitoring system (SHMS) deployed on the bridge, the difference of the wind turbulence characteristics under typhoons and normal wind is first identified, and the vibration energy distribution of the bridge responses under ten typical typhoons is analyzed using the wavelet packet method and compared with that under normal wind action. In addition, the PP and SSI-DATA methods are applied for the identification of modal parameters of the bridge under the long-lived typhoon Jongdari.

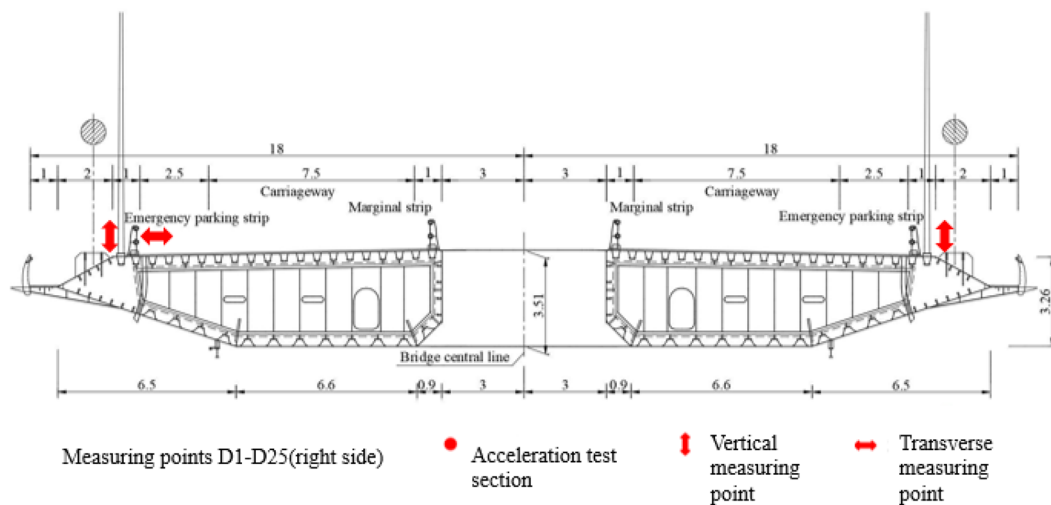
2 The instrumented bridge and monitoring data pre-processing

The Zhoushan islands–mainland connecting project [31, 32] aims to link Zhoushan Islands and Ningbo City in Zhejiang Province near the East China Sea. The Xihoumen Bridge is one of the five sea-crossing bridges in this project. As illustrated in Fig. 1a, the bridge in suspension form stretches from the southern Jintang Island to the northern Cezi Island. The total length of the bridge is 578 m + 1650 m + 485 m (Fig. 1a). The bridge girder is designed as twin-box structure as shown in Fig. 1b to resist strong winds in this region. The horizontal distance between the two boxes is 6 m, the width is 36 m, and the height is 3.5 m.

The Xihoumen Bridge was officially opened to traffic on December 25, 2009. A long-term SHMS was deployed since then to monitor the bridge condition in real time [33]. In



(a) General layout of Xihoumen Bridge



(b) Cross section of steel box girder

Fig. 1 The suspension Xihoumen Bridge (dimension: m)

this SHMS, nine uniaxial accelerometers were installed at 1/2, 1/4, and 3/4 main span inside the steel box girder and an ultrasonic anemometer was installed at 1/2 main span on the left side. The deployment of the accelerometers and ultrasonic anemometer is shown in Fig. 2, and the sampling frequencies of different sensors are listed in Table 1.

Due to its special geographical situation, the site of the Xihoumen Bridge is significantly affected by normal winds (monsoons) of small intensities and typhoons (tropical cyclones) of large intensities. During July–October every year, the Xihoumen Bridge is hit by typhoons at a high frequency. Different from normal winds, typhoons have obvious regional differences and strong specificity. In addition, there is a big difference in wind-induced bridge response characteristics due to the difference of aerodynamic features between typhoons and normal winds (monsoons). Therefore, it is of great significance to study the vibration energy distribution under typhoons and normal winds and to identify the

modal parameters of the bridge under typhoon excitations. In 2018, there were more than five typhoons affecting the bridge site in large scales. Among them the typhoon Jongdari was a typical long-lived one as shown in Fig. 3.

Acceleration and wind data collected by the deployed sensors are often subject to various environmental influences such as temperature, humidity, traffic, and electromagnetic interference, which make the data distorted [34, 35]. Figure 4 shows the 20 h of acceleration data collected from the bridge girder during the typhoon Jongdari on August 3, 2018. A number of spikes are observed in the time series shown in Fig. 4 due to the external interference. In this study, the abnormal spikes corrupted in the monitoring data were removed by the well-known Pauta criterion. According to this criterion, the sample points with instantaneous absolute values greater than three times the standard deviation in the measured data are removed. Then the linear interpolation method is used to interpolate the missing data position

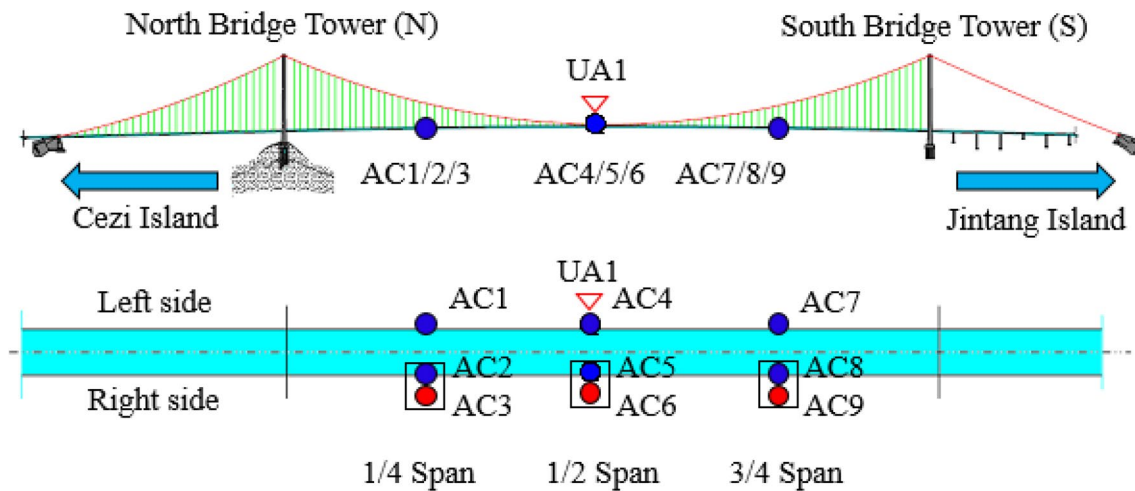


Fig. 2 Layout of accelerometers and anemometer

Table 1 Type and deployment locations of sensors

Sensor	Location	Sampling frequency (Hz)
Ultrasonic anemometer	UA1 (left side)	32
Uniaxial accelerometer (vertical)	AC1/4/7 (left side) AC2/5/8 (right side)	50
Uniaxial accelerometer (lateral)	AC3/6/9 (right side)	50



Fig. 3 Path map of the typhoon Jongdari

after removing the abnormal values. In addition, denoising is carried out to refine the raw acceleration data. There are numerous denoising methods for monitoring data, such as the Wiener filter, Kalman filter, adaptive filter, and wavelet denoising. Wavelet analysis has great advantages in the application of stationary and non-stationary signal denoising and can achieve good results [36–39]. In this study, the wavelet threshold denoising procedure [12, 37] is adopted to further process the acceleration data in order to eliminate the influence of high-frequency noise. The acceleration time histories during the typhoon Jongdari after removing abnormal

spikes and denoising are illustrated in Fig. 5. Figure 6 shows the frequency spectrum of raw and denoised acceleration data. It can be seen that the difference in frequencies of the dominate vibration modes are within 1 Hz and the difference in frequency spectrum is very small before and after the spike removing and the denoising. The other monitoring data used in this study are pre-processed in the same way.

3 Vibration energy distribution of wind-induced bridge responses

3.1 Analysis of wind field features

The difference of wind field features between typhoons and normal winds often leads to a significant difference in wind-induced dynamic response characteristics. We try to grasp this difference of dynamic response characteristics through comparing the vibration energy distribution when the bridge is subjected to typhoons and normal winds, respectively. Table 2 provides the maximum wind speeds, typhoon intensity levels and typhoon signaling numbers of ten typical typhoons, and a typical segment of normal wind, during which the wind and bridge response data collected will be used in the following study.

Among the ten typical typhoons in Table 2, the typhoon Jongdari and Chan-hom landed in Zhoushan, which was close to the site of Xihoumen Bridge and had a significant impact on the bridge. Therefore, the 20-h continuous wind data collected by the ultrasonic anemometer during the typhoon Jongdari and typhoon Chan-hom are used to comprehend the difference of turbulence characteristics between typhoons and normal winds. The comparison is made in terms of key turbulence characteristics such as turbulence intensity, gust factor, and fluctuating wind power spectral

Fig. 4 Raw data of accelerations collected at **a** AC4, **b** AC6, and **c** AC5

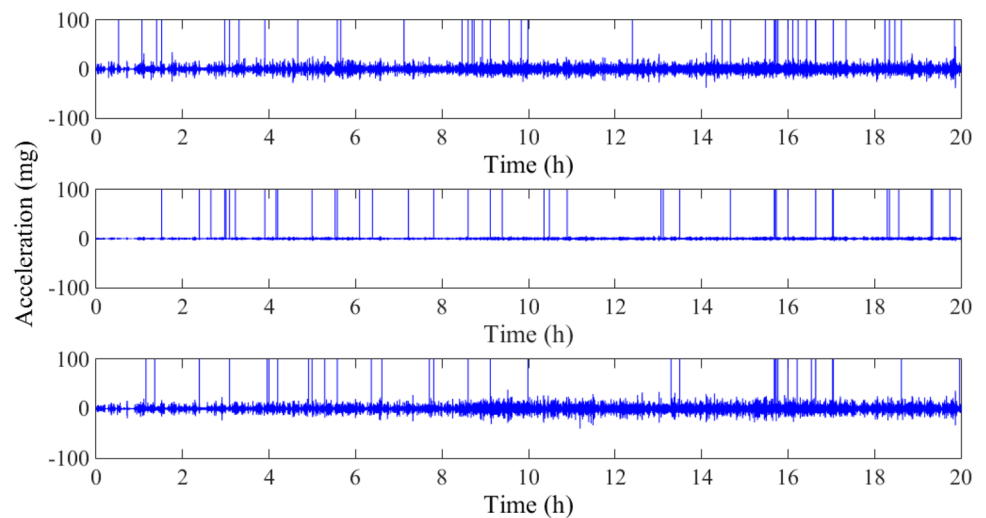
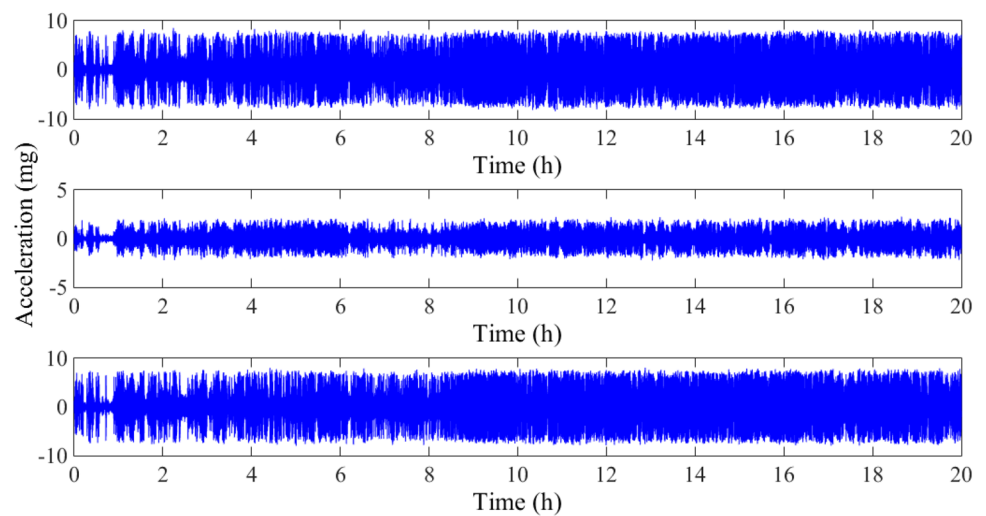


Fig. 5 Denoised data of accelerations at **a** AC4, **b** AC6, and **c** AC5



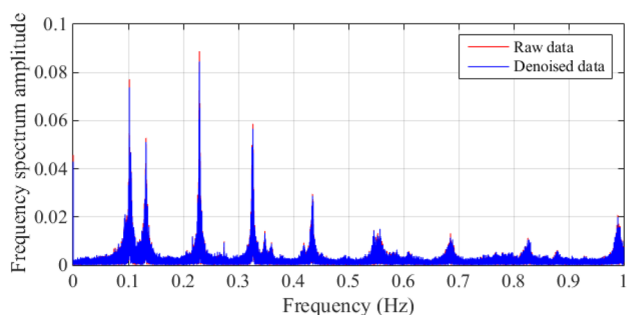
density (PSD). The obtained turbulence intensity, gust factor, and fluctuating wind PSD during typhoon Jongdari, typhoon Chan-hom, and normal wind are shown in Figs. 7, 8, and 9 and Tables 3 and 4.

It is seen in Figs. 7, 8, and 9 that the typhoons give rise to larger turbulence intensity, gust factor, and fluctuating energy than the normal wind. In addition, the energy of fluctuating wind during either typhoons or normal wind is larger in low-frequency band than in high-frequency band. Furthermore, it is observed that in the low-frequency range, the fluctuating wind energy of the typhoons change greatly, while that of the normal wind changes little.

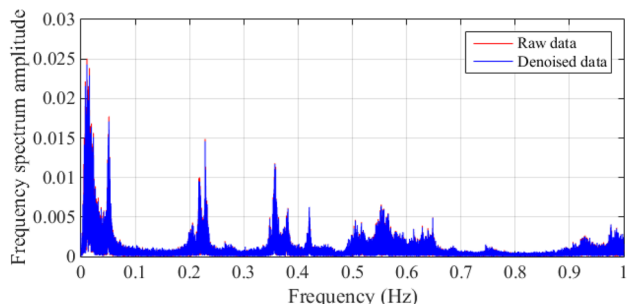
3.2 Analysis of vibration energy distribution

Since the fundamental frequencies of a long span suspension bridge are quite low, the bridge is easy to resonate in the low-frequency range with large fluctuating wind energy under wind excitations, which potentially brings about large

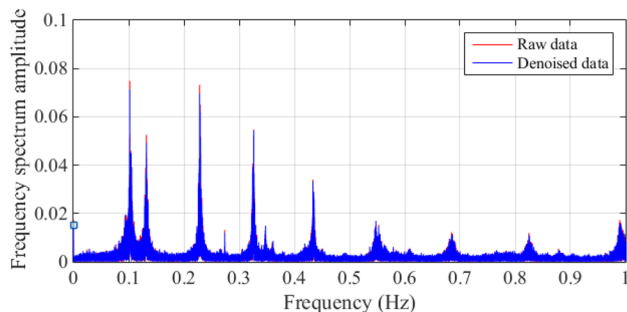
acceleration of the bridge and poses a threat to bridge safety. Therefore, it is desirable to evaluate the vibration energy distribution of the bridge under typhoons and normal winds in the low-frequency range. The vibration energy distribution of the Xihoumen Bridge is evaluated by use of the collected data during the ten typical typhoons and the normal wind (20 h for each). Since typhoon excitation is typically a nonstationary stochastic process, wavelet packet is utilized to conduct the signal processing due to its high resolution in both low- and high-frequency ranges. The wavelet packet is also applicable to the analysis of vibration energy distribution under normal winds. In this study, Daubechies-8 wavelet (DB8) is selected as the mother wavelet for basis function construction since it has been widely used for this purpose [12, 40]. The acceleration signals pre-processed in the previous section are first decomposed into four layers of wavelet packets. Then the wavelet packet coefficients are extracted, and the signals are reconstructed in the decomposed 16 frequency bands. Finally, the ratio of the energy



(a) AC4



(b) AC6



(c) AC5

Fig. 6 Comparison of frequency spectrum

in each frequency band to the total energy is calculated in order.

Assuming the sampling frequency of a vibration signal is f (50 Hz in this study), the frequency range analyzed is 0 to $f/2$. The pre-processed acceleration signal S is decomposed into i layers by wavelet packet, and thus 2^i sub-bands can be obtained. The signal can then be expressed by

$$S = \sum_{j=0}^{2^i-1} S_{i,j} = S_{i,0} + S_{i,1} + \dots + S_{i,j}, \tag{1}$$

where i is the total number of layers for wavelet packet decomposition, and $S_{i,j}$ is the reconstructed signal at the j th node of the i th layer.

According to the Parseval theorem in signal spectrum analysis, the energy of the signal component in the i th layer can be estimated as

$$E = \sum_{j=0}^{2^i-1} E_{i,j} = \sum_{j=0}^{2^i-1} \int |S_{i,j}|^2 dt = \sum_{j=0}^{2^i-1} \left(\sum_{k=1}^m |A_{j,k}|^2 \right), \tag{2}$$

where m is the number of discrete sampling points, $E_{i,j}$ represents the energy of the wavelet packet band at the j th node of the i th layer, and $A_{j,k}$ is the amplitude of the reconstructed signal $S_{i,j}$. The total energy E is the sum of the energy of each node signal component in the i th layer. The ratio of the energy of each frequency band to the total energy E can be obtained by

$$e_{i,j} = \frac{E_{i,j}}{E} \times 100\% . \tag{3}$$

The schematic diagram of wavelet packet decomposition of the acceleration signal is shown in Fig. 10. According to Eqs. (1)–(3), the vertical vibration energy distributions at 1/2, 1/4, and 3/4 main span at the left girder are obtained as shown in Fig. 11. It can be observed that the vibration energy during the ten typhoons is mainly distributed over the first three frequency bands, and the energy proportion in higher frequency bands is close to zero. Table 5 compares the average energy proportion of the first three frequency bands at different locations.

It is found from Fig. 11 and Table 5 that the vibration energy distribution over the first three frequency bands possesses more than 95% of the total energy under typhoons. The energy distributions of different typhoons are similar, and the dynamic responses at the three locations (1/4, 1/2, and 3/4 main span) generate similar energy distribution trends with about 76%, 10%, and 10% proportion in the first three bands, respectively. The energy proportion among the three frequency bands under typhoons conforms to a nearly identical ratio of 1:0.14:0.14 for all three locations. Therefore, special attention should be paid to the low-frequency ingredients of typhoons when hitting a long span suspension bridge.

Typhoons have the characteristics of high wind speed and strong specificity, and their wind speed and intensity are significantly distinct from normal winds, as shown in Table 2. Also, the fluctuation characteristics of typhoons and normal winds are different, as illustrated in Figs. 7, 8, and 9. Furthermore, the low wind speed in normal winds may bring vortex-induced vibration to bridge girder, while the high wind speed in typhoons may bring flutter and other aerodynamic phenomena on the bridge. The difference of wind natures between typhoons and normal winds makes it important to evaluate the difference in bridge dynamic response characteristics under typhoons and normal winds,

Table 2 Information of ten typhoons and normal wind

Number	Name	Intensity level	Maximum wind speed (m/s)	Number	Name	Intensity level	Maximum wind speed (m/s)
2013 No. 7	Soulik	Super typhoon	31.69	2016 No. 14	Meranti	Super typhoon	28.14
2013 No. 23	Fitow	Strong typhoon	30.53	2017 No. 9	Nesat	Tropical storm	27.22
2014 No. 10	Matmo	Strong typhoon	28.33	2017 No. 18	Talim	Tropical storm	26.20
2014 No. 16	Fung-wong	Tropical storm	38.97	2018 No. 12	Jongdari	Tropical storm	24.31
2015 No. 9	Chan-hom	Super typhoon	41.21	2018	Normal wind	Normal wind	10.35
2015 No. 21	Dujuan	Super typhoon	21.90				

Fig. 7 Turbulence intensity

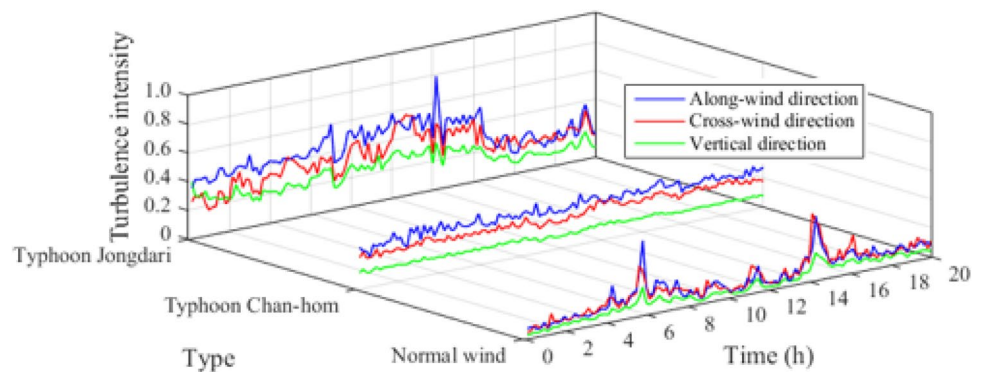
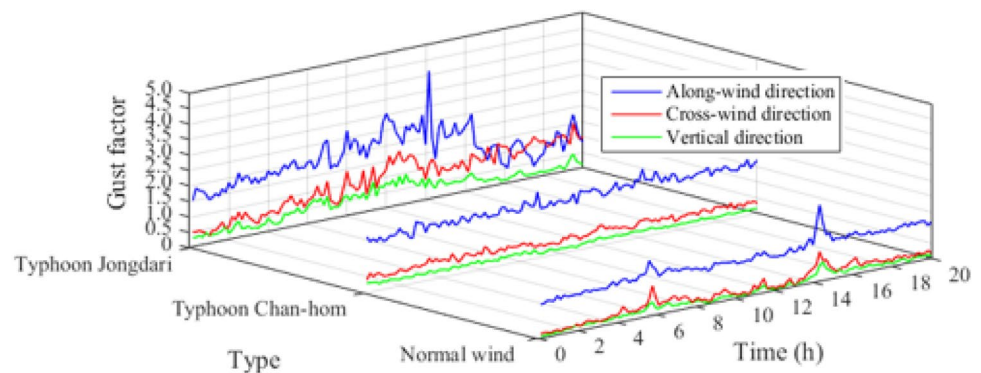


Fig. 8 Gust factor



and vibration energy distribution is one of such dynamic response characteristics. Table 6 lists the vibration energy distribution of the bridge response under normal wind, and Fig. 12 compares the energy distributions in each frequency band under typhoons and normal wind. In Fig. 12, the energy proportions in relation to typhoons at different spans are the average values obtained from the ten typhoons.

It can be seen from Tables 5 and 6 and Fig. 12 that the energy proportion under typhoons in the first frequency band is the largest accounting for about 80% of the total energy,

and the energy proportion in the second and third frequency bands is nearly accounting for 10% of the total energy. Under normal wind, the energy proportion is evenly distributed in the first three bands with about 90% proportion in total, and the energy proportion in the fourth band is small. It is worth mentioning that the energy proportion of different frequency bands from responses at 1/4, 1/2, and 3/4 main span is similar under typhoons, but different under normal wind, which is mainly manifested in the difference of the range of frequency band with the largest energy proportion. The

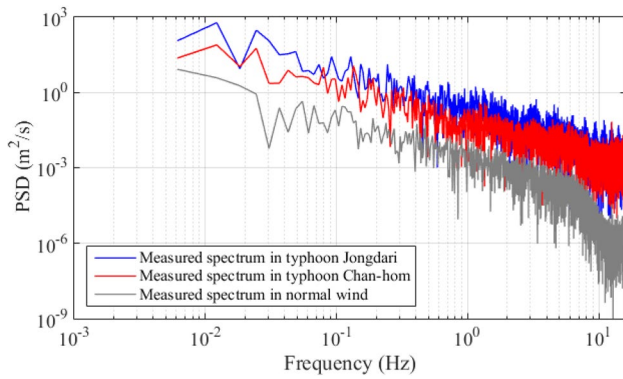


Fig. 9 Fluctuating wind (along-wind) PSD during typhoons and normal wind

Table 3 Mean turbulence intensity

Type	Turbulence intensity		
	Along-wind	Cross-wind	Vertical
Typhoon Jongdari	0.4120	0.3090	0.1854
Typhoon Chan-hom	0.2802	0.2174	0.0979
Normal wind	0.1423	0.1272	0.0686

Table 4 Mean gust factor

Type	Turbulence intensity		
	Along-wind	Cross-wind	Vertical
Typhoon Jongdari	1.7377	0.5006	0.3447
Typhoon Chan-hom	1.7046	0.4612	0.1961
Normal wind	1.2968	0.2992	0.1719

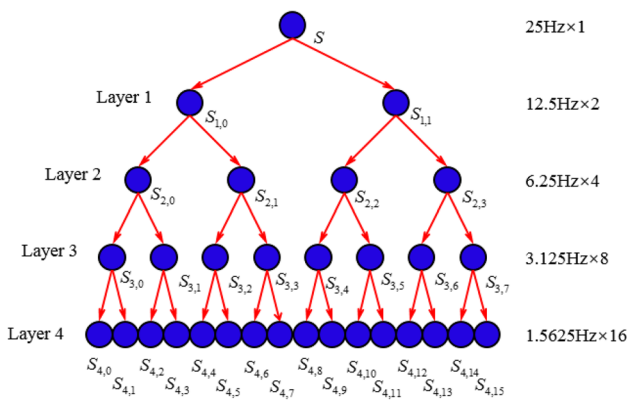
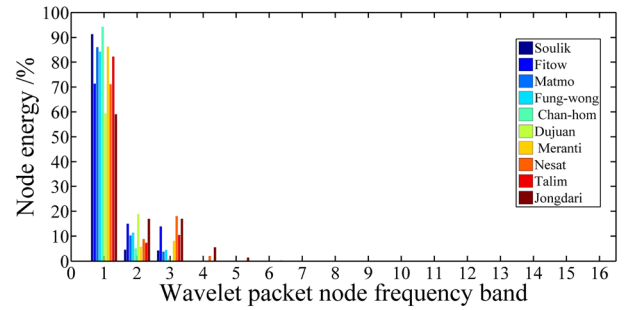
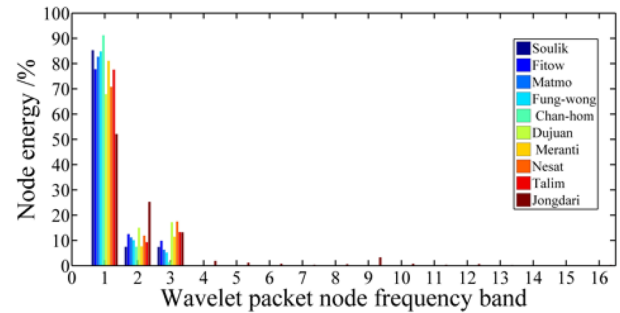


Fig. 10 Wavelet packet decomposition of a signal

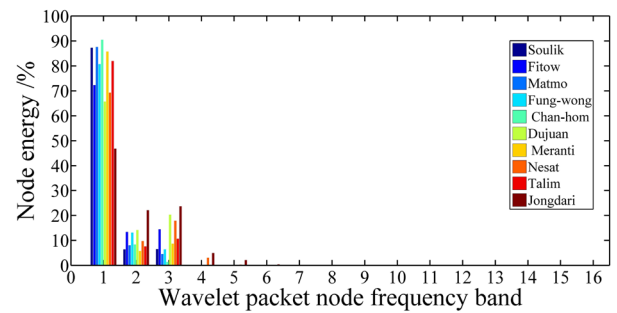
frequency band with the largest energy proportion for the 1/2 main span under normal winds is the third frequency band, but the frequency band with the largest energy proportion



(a) At 1/2 span



(b) At 1/4 span



(c) At 3/4 span

Fig. 11 Energy distribution at 16 bands under ten typhoons

Table 5 Average energy proportion of first three frequency bands at different locations

Location	Average energy proportion (%)		
	1st band (0–1.5625 Hz)	2nd band (1.5625– 3.125 Hz)	3rd band (3.125– 4.6875 Hz)
1/2 span	78.48	10.35	8.03
1/4 span	77.08	11.73	10.22
3/4 span	76.71	10.8	11.37

for the 1/4 and 3/4 main span is the first band under normal winds. In addition, the energy proportion in the first frequency band under normal winds is about 40% of that

Table 6 Energy proportion of first four frequency bands under normal wind

Location	Energy proportion (%)			
	1st band	2nd band	3rd band	4th band
1/2 span	25.63	28.41	38.53	6.74
1/4 span	31.01	27.66	29.1	2.2
3/4 span	37.64	22.79	31.59	7.18

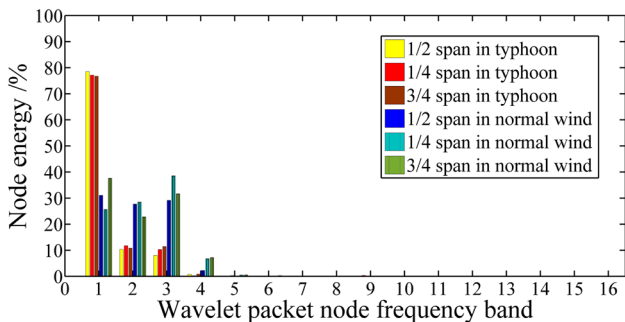


Fig. 12 Comparison of energy distributions under typhoon and normal wind

under typhoons, while the energy proportion in the second and third frequency bands under normal winds (about 30% each) is about three times that under typhoons (about 10% each). It is known from Fig. 9 that in the same range of low-frequency band, the fluctuating wind energy under normal wind changes little, while that under typhoons change greatly. The difference of wind energy in the low-frequency band contributes largely to the difference in wind-induced dynamic response. Based on the difference of energy distribution in different frequency bands under typhoons and normal winds, we gain insight into the influence of typhoons on bridge dynamic responses in different frequency bands.

Since a large amount of vibration energy is concentrated in the low-frequency bands under wind excitations especially typhoons, identification of the low-order modal parameters of the bridge under typhoons is of great significance for vibration suppression and structural condition evaluation.

4 Modal parameter identification using typhoon-induced dynamic responses

4.1 Modal parameter identification methods

The modal parameters of the Xihoumen Bridge are identified by the peak picking (PP) method and the stochastic subspace identification (SSI) method using the bridge dynamic responses acquired during typhoons. Theoretically, the PP method estimates the modal frequencies by observing the

peak values of frequency response function. However, since the accurate input (distributed wind loads) is unknown for a long-span bridge, it is impossible to obtain the frequency response function in practice. If the wind excitation can be considered as a random white noise and its amplitude distribution satisfies the normal distribution, then the self-power spectral density function of the input signal is a constant. Under this assumption, the self-power spectral density function of the output signal also reaches peak values at the characteristic frequency points [23], that is

$$G_{yy}(j\omega_i) = H^*(j\omega_i)G_{xx}(j\omega_i)H^T(j\omega_i) = \frac{R_i^* C^T R_i}{\sigma_i} = \frac{\phi_i^* \gamma_i^H C \gamma_i \phi_i^T}{(\sigma_i)^2} = \alpha_i \phi_i^* \phi_i^T, \tag{4}$$

where α_i is a constant, i is the number of output channels, G_{yy} and G_{xx} are the power spectral density functions of the output and input, respectively. $R_i = \phi_i \gamma_i^T$, ϕ_i is mode vector, and γ_i is the mode participation vector.

In the PP method, the damping ratios of the structure are identified by the half-power bandwidth method [41]. A peak value appears at the corresponding characteristic frequency f_i with amplitude A_i . The frequencies at the horizon of $A_i/\sqrt{2}$ are denoted as f_{h1} and f_{h2} . With these two half-power points, the damping ratio associated with the characteristic frequency f_i can be obtained as [41]

$$\xi_i = \frac{f_{h2} - f_{h1}}{2f_i}, \tag{5}$$

The stochastic subspace identification (SSI) approach can be categorized as data-driven SSI (SSI-DATA) method and covariance-driven SSI (SSI-COV) method. The two methods have similar identification accuracy, but the SSI-DATA method is superior to the SSI-COV method in regard to computational efficiency and configuration requirement. Therefore, the SSI-DATA method is used in this study.

The SSI approach proceeds in general first to construct the Hankel matrix and then to divide the response matrix into the past and future blocks [35]. The SSI-DATA method decomposes the Hankel matrix by QR decomposition, where the Hankel matrix is expressed to comprise the past and future blocks [42]

$$H = \frac{1}{\sqrt{n}} \begin{bmatrix} y_0 & y_1 & \dots & y_{n-1} \\ y_1 & y_2 & \dots & y_n \\ \vdots & \vdots & \ddots & \vdots \\ y_{i-1} & y_i & \dots & y_{i+n-2} \\ y_i & y_{i+1} & \dots & y_{i+n-1} \\ y_{i+1} & y_{i+2} & \dots & y_{i+n} \\ \vdots & \vdots & \ddots & \vdots \\ y_{2i-1} & y_{2i} & \dots & y_{2i+n-2} \end{bmatrix} = \begin{bmatrix} Y_{0|i-1} \\ Y_{i|2i-1} \end{bmatrix} = \begin{bmatrix} Y_p \\ Y_f \end{bmatrix} = \begin{matrix} \text{past} \\ \text{future} \end{matrix}, \tag{6}$$

where n is the number of matrix columns, y_i is the output data at the i th measurement point, Y_p is the past response matrix (block), s and Y_f is the future response matrix (block).

The future response matrix is projected onto the past response matrix to obtain the projection matrix by orthogonal projection. Then the observation matrix and Kalman filtering vector are obtained by singular value decomposition of the projection matrix, from which the characteristic matrix and output matrix are elicited to identify the modal frequencies, damping ratios, and mode shapes. The modal frequencies and damping ratios obtained by the SSI-DATA method can be expressed as [42]

$$f_i = \frac{\sqrt{a_i^2 + b_i^2}}{2\pi}, \tag{7}$$

$$\xi_i = \frac{-a_i}{\sqrt{a_i^2 + b_i^2}}, \tag{8}$$

where $\lambda_i^c = a_i \pm jb_i$, λ_i^c is the i th eigenvalue of the system matrix of the structure, f_i is the modal frequency (Hz), and ξ_i is the damping ratio.

4.2 Modal parameters identified by the PP method

The PP method is first applied to estimate the power spectral density (PSD) functions of the acceleration responses at the 1/2 span measured during the long-lived typhoon Jongdari. The power spectra of the vertical responses at the left and right girders are illustrated in Figs. 13 and 14, while Fig. 15 shows the power spectrum of the lateral response at the right girder.

Since the fundamental frequencies of a long-span suspension bridge are in general extremely low and the first mode has its frequency much less than 1 Hz, the PSD function in the range of 0–1 Hz is considered in the modal identification. As shown in Figs. 13 and 14, the peak frequencies obtained from the left and right girders at the 1/2 span in the vertical direction match well with each other. It is seen from Fig. 15

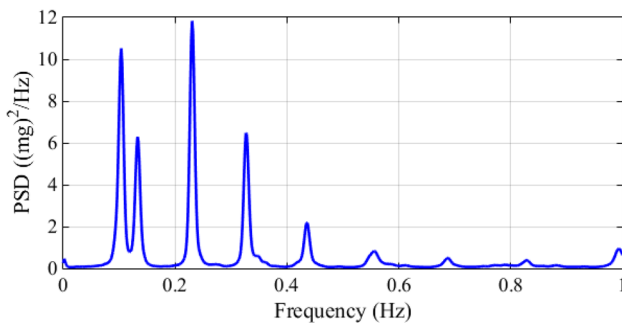


Fig. 13 PSD of vertical acceleration of 1/2 span at left side

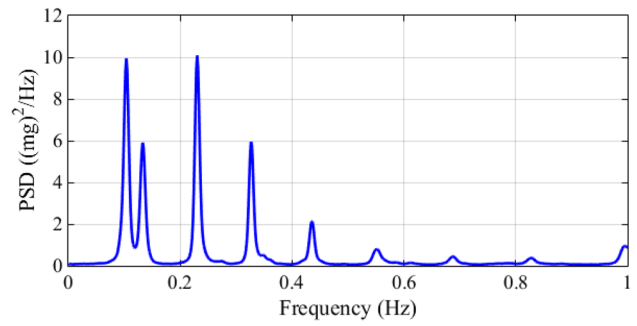


Fig. 14 PSD of vertical acceleration of 1/2 span at right side

that the lateral frequencies obtained from the response at the 1/2 span are mainly concentrated in 0 to 0.5 Hz.

4.3 Modal parameters identified by SSI-DATA method

The SSI-DATA method deals with the measured acceleration data directly in the time domain, thus having better signal to noise ratio (SNR) in data processing. Also, because the SSI-DATA method uses an overall fitting approach when calculating the minimum implementation of the system, it is efficient in handling dense modes. One main challenge in the SSI-DATA method is the estimation of system (modal) order. A traditional procedure is to determine the system order according to the number of non-zero values in the singular value matrix. In practice, however, the higher-order singular values may not be zero due to the existence of noise. In this case, the modal order can be estimated by observing jump in the singular value sequence. If there is a jump in the singular value sequence, half number of the singular values before the jump point can be considered as the system (modal) order. Figure 16 shows the singular value diagram of the lateral acceleration at the 1/2 span during the typhoon Jongdari. Although several jumps are observed, the singular values at these jump locations are still quite large (much higher than 1.0).

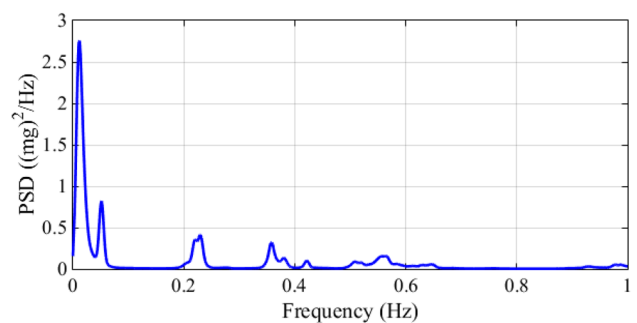


Fig. 15 PSD of lateral acceleration of 1/2 span at right side

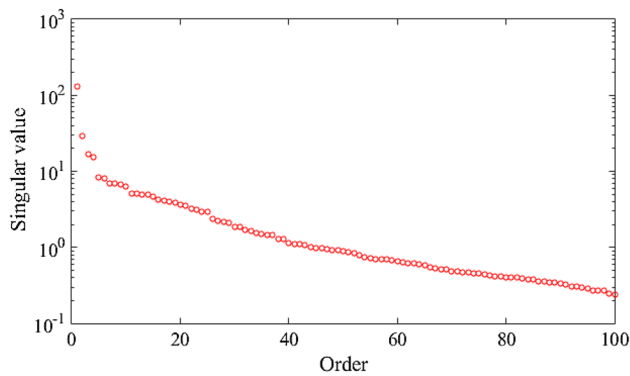


Fig. 16 Singular value diagram

Since it is difficult to determine the system (modal) order from the singular value diagram in our case, the stability diagram method is adopted hereafter to identify the modal parameters of the bridge. The stability diagram method [42, 43] assumes that the system has N_{\min} to N_{\max} modal orders, then N (N_{\min} to N_{\max}) stochastic state-space models are obtained. The modal parameters of each state-space model are identified and plotted in the Cartesian coordinate system, in which the abscissa denotes modal frequency and the ordinate represents modal order. If the error of the frequency and damping ratio between two critical points is within the allowable range, then they will be considered as stable points. The stable points at each modal frequency location will form a stable axis, thus the modal parameters of each order can be obtained. Figures 17 and 18 illustrate the stability diagrams of the vertical and lateral accelerations obtained during the typhoon Jongdari. The modal frequencies of the bridge are then determined by the stable axes.

It can be seen from Figs. 17 and 18 that the stability diagram of the vertical acceleration is more stable than that of the lateral acceleration, and the stabilization axes of the former are clearer. There are many disordered points in the stability diagram of the lateral acceleration, which indicates that the lateral acceleration is polluted with more noise.

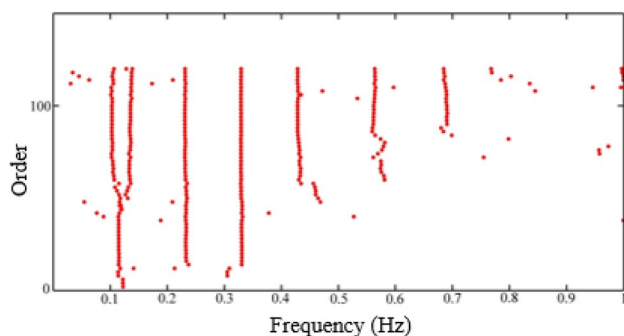


Fig. 17 Stability diagram of vertical acceleration

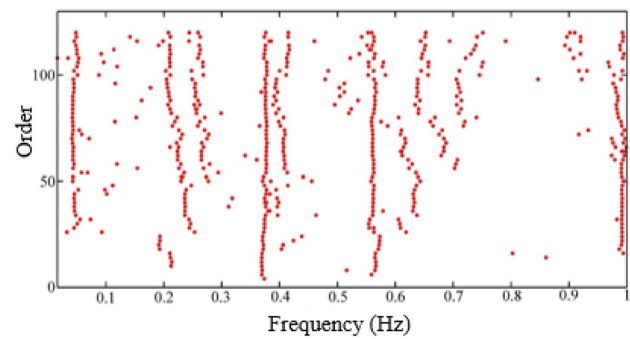


Fig. 18 Stability diagram of lateral acceleration

4.4 Comparison of Identified modal frequencies and damping ratios

The modal frequencies and damping ratios identified by the PP and SSI-DATA methods using the acceleration responses acquired during the typhoon Jongdari are compared to the benchmark results, which were obtained during the ambient vibration testing immediately after the construction of the bridge and before being open to traffic. Tables 7 and 8 provide the vertical and lateral modal parameters (modal frequencies and damping ratios) of the bridge.

It is observed from Table 7 that for vertical modes, the modal frequencies' identification results by the PP and SSI-DATA methods agree well with each other, and both of them are in coincidence with the benchmark results. The modal damping ratios identification results by the PP method are significantly larger than those obtained by the SSI-DATA method, and the latter are favorably in agreement with the benchmark results (the response level under typhoon excitation is greatly higher than that under ambient vibration excitation, and a higher level of responses in general arouses more damping). As far as the lateral modes are concerned in Table 8, it is found that the modal frequencies' identification results by SSI-DATA method are generally in agreement with the benchmarks. While the PP method leads to mismatch in the modal frequencies identification. In addition, the first two order modal frequencies identified by PP and SSI-DATA methods error is relatively large, which may be caused by nonlinear factors brought under typhoon Jongdari. Likewise, the damping ratios identified by the PP method deviate greatly from the benchmark results, while those identified by the SSI-DATA method are much closer to the benchmark results.

Both PP and SSI-DATA methods have high reliability in frequencies identification, but there are obvious differences in damping ratios identification. PP method is a frequency domain identification method and transforms the measured acceleration data under typhoon to the frequency domain through Fast Fourier Transform (FFT), but it is difficult to

Table 7 Vertical modal parameters identified by two methods

Mode No.	Modal frequency (Hz)			Damping ratio (%)		
	PP	SSI-DATA	Benchmark	PP	SSI-DATA	Benchmark
1	0.104	0.103	0.103	2.54	1.92	1.32
2	0.133	0.134	0.133	2.07	1.56	1.18
3	0.230	0.231	0.229	1.05	0.81	0.71
4	0.327	0.329	0.327	1.16	0.39	0.52
5	0.436	0.428	0.435	0.65	0.36	0.29
6	0.552	0.562	0.549	1.07	0.37	0.41

Table 8 Lateral modal parameters identified by two methods

Mode No.	Modal frequency (Hz)			Damping ratio (%)		
	PP	SSI-DATA	Benchmark	PP	SSI-DATA	Benchmark
1	0.0392	0.0420	0.0540	4.05	2.88	2.10
2	0.0520	0.211	0.123	2.79	1.61	2.10
3	0.240	0.253	0.260	1.40	0.70	0.86
4	0.359	0.372	0.372	1.38	0.42	0.65
5	0.423	0.406	0.399	0.72	0.45	0.56
6	0.565	0.560	0.601	0.45	0.23	0.15

find the half power point from the FFT spectrum. Generally, the half power point is approximately determined by linear interpolation to calculate the damping ratios. Moreover, FFT in PP method is easy to cause truncation error which makes PP method inaccurate in damping ratios identification [44, 45], while the SSI-DATA method is a time domain identification method that overcomes the shortcomings of frequency-domain identification method such as PP method. Therefore, the SSI-DATA lead to the identification results with higher accuracy.

In summary, when using typhoon-induced dynamic responses, the SSI-DATA method achieves in general better estimates of modal frequencies and damping ratios than the PP method. Nevertheless, it is worth recalling that the SSI-DATA method relies on the assumption of random white-noise excitations, yet the excitation during a strong typhoon maybe non-white and non-stationary. Furthermore, under the action of a strong typhoon, local nonlinear behaviors may appear in a long-span bridge, and this nonlinearity would give rise to errors in modal identification. These critical factors require further exploration to obtain more accurate structural modal information of the actual bridge and this will be the work in the future.

5 Conclusions

This paper presented a study on the wind turbulence characteristics, vibration energy distribution, and modal properties of a long-span suspension bridge under typhoon and normal wind (monsoon) conditions. The wind and

acceleration data during ten typical typhoons and normal wind, collected by an online structural health monitoring system deployed on the bridge, were used in the study. The results obtained from this study provided a reference baseline for structural condition assessment and vibration mitigation of the bridge in the future typhoons. The present study draws the following conclusions:

- 1) The wind field characteristics and the vibration energy distribution during typhoons and normal wind are distinct. In the low-frequency range, the fluctuating wind energy of typhoons changes more significantly than that of normal winds. The energy under typhoons is mainly concentrated in the first frequency band with more than 80% proportion, while the energy under normal winds is evenly distributed in the first three frequency bands with about 90% proportion in total.
- 2) The vibration energy distributions of the dynamic responses at the locations of 1/4, 1/2, and 3/4 main span are similar under typhoons but different under normal winds, which is mainly manifested in the difference of the range of frequency band with the largest energy proportion. In view of this, much attention should be paid to the vibration risk caused by the first frequency band under typhoons while the vibration risk under normal winds should consider a larger frequency range.
- 3) When using typhoon-induced dynamic responses for modal identification, the PP method may result in a distortion in modal frequencies and largely overestimate damping ratios while the SSI-DATA method performs

much better for both modal frequencies and damping ratios.

Acknowledgements The authors greatly appreciate reviewers for their valuable advices for improving the quality of this paper. The authors also thank the financial support in this paper granted by the National Key Research and Development Program of China (2018YFC0809604), the Key Research and Development Program of Zhejiang (2019C03098) and the National Natural Science Foundation of China (U1709207, 52078461, 51578506).

References

- Chou JM, Dong WJ, Tu G, Xu Y (2020) Spatiotemporal distribution of landing tropical cyclones and disaster impact analysis in coastal China during 1990–2016. *Phys Chem Earth Parts A/B/C* 115:102830. <https://doi.org/10.1016/j.pce.2019.102830>
- Zhang Y, Wei K, Zw S, Bai XW, Lu XZ, Soares CG (2020) Economic impact of typhoon-induced wind disasters on port operations: a case study of ports in China. *Int J Disaster Risk Reduct* 50:101719. <https://doi.org/10.1016/j.ijdrr.2020.101719>
- Zhou Y, Sun LM (2018) Effects of high winds on a long-span sea-crossing bridge based on structural health monitoring. *J Wind Eng Ind Aerodyn* 174:260–268. <https://doi.org/10.1016/j.jweia.2018.01.001>
- Chen Y, Duan ZD (2018) A statistical dynamics track model of tropical cyclones for assessing typhoon wind hazard in the coast of southeast China. *J Wind Eng Ind Aerodyn* 172:325–340. <https://doi.org/10.1016/j.jweia.2017.11.014>
- Huang MF, Xu Q, Xu HW, Ni YQ, Kwok K (2018) Probabilistic assessment of vibration exceedance for a full-scale tall building under typhoon conditions. *Struct Des Tall and Sp Build*. <https://doi.org/10.1002/tal.1516>
- Guo J, Hang D, Zhu XJ (2020) Prediction of crack propagation in U-rib components based on the Markov Chain. *J Bridge Eng* 25(10):1–9. [https://doi.org/10.1061/\(ASCE\)BE.1943-5592.0001624](https://doi.org/10.1061/(ASCE)BE.1943-5592.0001624)
- Guo J, Zhu MJ (2020) Static aerodynamic force coefficients analysis of the girder in the arch bridge sea-crossing. *Wind and Struct* (Accepted)
- Zhang YC, Fan JP, Deng H (2013) Forecasting of typhoon disaster loss in Zhejiang Province based on the combination forecasting model. *J Nat Disasters* 22(6):223–231. <https://doi.org/10.13577/j.jnd.2003.0630>
- Ding YL, Li AQ, Deng Y (2010) Structural damage warning of a long-span cable-stayed bridge using novelty detection technique based on wavelet packet analysis. *Adv Struct Eng* 13(2):291–298. <https://doi.org/10.1260/1369-4332.13.2.291>
- Ge JP, Li HS (2011) Experiment on damage detection of girder bridge using wavelet packet energy accumulated variation. *J Vib Meas Diagn* 31(1):85–88. <https://doi.org/10.1080/0144929X.2011.553739>
- Wei YM, Zhang YZ, Wang T, Yang Z (2017) Damage identification based on structural dynamic responses using wavelet packet energy eigenvector. *China Earthq Eng J* 39(06):1156–1160. <https://doi.org/10.3969/j.issn.1000-0844.2017.06.1156>
- Guo J, He JX (2020) Dynamics response analysis of ship-bridge collisions experiment. *J Zhejiang Univ Sci A (Appl Phys Eng)* 21(7):525–534. <https://doi.org/10.1631/jzus.A1900382>
- Pan Y, Zhang LM, Wu XG, Zhang KN, Skibniewski MJ (2019) Structural health monitoring and assessment using wavelet packet energy spectrum. *Saf Sci* 120:652–665. <https://doi.org/10.1016/j.ssci.2019.08.015>
- Peeters B, Maeck J, Roeck GD (2001) Vibration-based damage detection in civil engineering: excitation sources and temperature effects. *Smart Mater Struct* 10(3):518–527. <https://doi.org/10.1088/0964-1726/10/3/314>
- Ren WX, Zong ZH (2004) Output-only modal parameter identification of civil engineering structures. *Structural Engineering and Mechanics* 17(3–4):429–444. https://doi.org/10.12989/sem.2004.17.3_4.429
- Ren WX, Zhao T, Harik IE (2004) Experimental and analytical modal analysis of steel arch bridge. *J Struct Eng* 130(7):1022–1031. [https://doi.org/10.1061/\(ASCE\)0733-9445\(2004\)130:7\(1022\)](https://doi.org/10.1061/(ASCE)0733-9445(2004)130:7(1022))
- Weng JH, Loh CH, Lynch JP, Lu KC, Lin PY, Wang Y (2008) Output-only modal identification of a cable-stayed bridge using wireless monitoring systems. *Eng Struct* 30(7):1820–1830. <https://doi.org/10.1016/j.engstruct.2007.12.002>
- Jang S, Jo H, Cho S, Mechitov K, Rice JA, Sim SH, Jung HJ, Yun CB, Spencer JBF, Agha G (2010) Structural health monitoring of a cable-stayed bridge using smart sensor technology: deployment and evaluation. *Smart StructSyst* 6(5–6):439–459. https://doi.org/10.12989/sss.2010.6.5_6.439
- Zarbat SEHAM, Norouzi M, Allemang RJ, Hunt VJ, Helmicki A, Nims DK (2017) Stay force estimation in cable-stayed bridges using stochastic subspace identification methods. *J Bridge Eng* 22(9):04017055. [https://doi.org/10.1061/\(ASCE\)BE.1943-5592.0001091](https://doi.org/10.1061/(ASCE)BE.1943-5592.0001091)
- Mao J, Wang H, Fu YG, Spencer BF (2019) Automated modal identification using principal component and cluster analysis: application to a long-span cable-stayed bridge. *Struct Control Health Monit* 26(10):e2430. <https://doi.org/10.1002/stc.2430>
- Wang H, Mao JX, Xu ZD (2020) Investigation of dynamic properties of a long-span cable-stayed bridge during typhoon events based on structural health monitoring. *J Wind Eng Ind Aerodyn* 210:104172. <https://doi.org/10.1016/j.jweia.2020.104172>
- Robson JD (1981) Engineering applications of correlation and spectral analysis. *J Sound Vib* 74(4):611–612. [https://doi.org/10.1016/0022-460X\(81\)90424-7](https://doi.org/10.1016/0022-460X(81)90424-7)
- Andersen P, Brincker R, Peeters B, Roeck GD, Hermans L, Kramer C (1998) Comparison of system identification methods using ambient bridge test data. *Proc SPIE Int Soc Opt Eng* 3727:1035–1041
- Zong ZH, Lai CL, Lin YQ, Ren WX (2004) Analysis of dynamic characteristics of a large-span prestressed concrete continuous rigid frame bridge. *J Earthq Eng Eng Vib* 24(3):98–104. <https://doi.org/10.13197/j.eeev.2004.03.013>
- Ye ZL, Li N, Zhang FJ (2019) Wind characteristics and responses of Xihoumen Bridge during typhoons based on field monitoring. *J Civ Struct Health Monit* 9(1):1–20. <https://doi.org/10.1007/s13349-019-00325-y>
- Wang H, Mao JX, Huang JH, Li AQ (2016) Modal identification of Sutong cable-stayed bridge during typhoon haikui using wavelet transform method. *J Perform Construct Fac* 30(5):04016001. [https://doi.org/10.1061/\(ASCE\)CF.1943-5509.0000856](https://doi.org/10.1061/(ASCE)CF.1943-5509.0000856)
- Sun Q, Yan WJ, Ren WX (2017) Operational modal analysis for bridge engineering based on the dynamic transmissibility measurements. *Eng Mech* 34(11):194–201. <https://doi.org/10.6052/j.issn.1000-4750.2016.07.0558>
- Zong ZH, Zhang K, Liao YC, Wu R (2019) Modal frequency identification of cable-stayed bridges considering uncertainties of operational environmental factors. *China J Highw Transp* 32(11):40–50. <https://doi.org/10.19721/j.cnki.1001-7372.2019.11.003>
- Wen P, Chen QF, Yang FF (2020) Modal parameter identification for large span cable-stayed bridge based on improved stochastic subspace identification. *J Chongqing Jiaotong Univ*

- (Natural Science) 39(1):45–50. <https://doi.org/10.3969/j.issn.1674-0696.2020.01.08>
30. Eshkevari SS, Pakzad SN, Takac M, Matarazzo TJ (2020) Modal identification of bridges using mobile sensors with sparse vibration data. *J Eng Mech* 146(4):1–18. <https://doi.org/10.3969/j.issn.1674-0696.2020.01.08>
 31. Song H, Wang X (2009) Overall design of Xihoumen Bridge in Zhoushan islands-to-mainland linking project. *Highway* 1:8–16
 32. Guo J (2010) Key technical innovation of Xihoumen Bridge-the longest steel box gird suspension bridge in the world. *Eng Sci* 8(4):18–22
 33. Hu J, Guo J, Ou JP (2011) Measurement of wind field characteristics at a long-span suspension bridge. *J Southeast Univ* 27(3):328–334. <https://doi.org/10.3969/j.issn.1003-7985.2011.03.020>
 34. Frangopol DM, Strauss A, Kim S (2008) Use of monitoring extreme data for the performance prediction of structures: general approach. *Eng Struct* 30(12):3644–3653. <https://doi.org/10.1016/j.engstruct.2008.06.010>
 35. Shao YF, Miao CQ, Li BW, Wu QD (2019) Simultaneous denoising and enhancement method for long-span bridge health monitoring data based on empirical mode decomposition and fractal conservation law. *Meas Sci Technol* 30(6):065103. <https://doi.org/10.1088/1361-6501/ab078c>
 36. Smith CB, Akopian D, Agaian SS (2004) Least squares optimization of a polynomial threshold for wavelet domain denoising. In: *The 7th International Conference on Signal Processing Proceedings, ICOSP*, pp 109–112. <https://doi.org/10.1109/ICOSP.2004.1452593>
 37. Guo J, Gu ZW, Sun BN, Chen Y (2006) Method of bridge health monitoring based on wavelet analysis. *Eng Mech* 23(12):129–135. <https://doi.org/10.3969/j.issn.1000-4750.2006.12.023>
 38. Ni YQ, Xia HW, Wong KY, Ko JM (2012) In-service condition assessment of bridge deck using long-term monitoring data of strain response. *J Bridge Eng ASCE* 17(6):876–885. [https://doi.org/10.1061/\(ASCE\)BE.1943-5592.0000321](https://doi.org/10.1061/(ASCE)BE.1943-5592.0000321)
 39. Xia YX, Ni YQ (2018) A wavelet-based despiking algorithm for large data of structural health monitoring. *Int J Distrib Sens Netw* 14(12):1550147718819095. <https://doi.org/10.1177/1550147718819095>
 40. Huang D, Cui S, Li XQ (2019) Wavelet packet analysis of blasting vibration signal of mountain tunnel. *Soil Dyn Earthq Eng* 117:72–80. <https://doi.org/10.1016/j.soildyn.2018.11.025>
 41. Li JZ, Yan JK, Peng TB, Han L (2015) Shake table studies of seismic structural systems of a Taizhou Changjiang Highway Bridge model. *J Bridge Eng* 20(3):04014065
 42. Peeters B, Roeck GD (2000) Reference based stochastic subspace identification in civil engineering. *Inverse Probl Eng* 8(1):47–74. <https://doi.org/10.1016/j.soildyn.2018.11.025>
 43. Chang J, Zhang QW, Sun LM (2007) Application of stabilization diagram for modal parameter identification using stochastic subspace method. *Eng Mech* 24(2):39–44. <https://doi.org/10.3969/j.issn.1000-4750.2007.02.007>
 44. Zhang ZY, Pan Q, Cho CD, Gao ZC (2009) Identification of damping ratios of soil-structure system subjected to ambient excitation. In: *Proc. of Int. Symp. on Geoenvironmental Eng., ISGE2009*, pp 492–496. <https://doi.org/10.1007/978-3-642-04460-143>
 45. Damir Z, Mirsad T, Radomir F (2015) Identification of modal parameters of bridges using ambient vibration measurements. *Shock Vib*. <https://doi.org/10.1155/2015/957841>

Publisher's Note Springer Nature remains neutral with regard to jurisdictional claims in published maps and institutional affiliations.